LETTER

Stable colloids in molten inorganic salts

Hao Zhang[1], Kinjal Dasbiswas[1], Nicholas B. Ludwig[1], Gang Han[2], Byeongdu Lee[3], Suri Vaikuntanathan[1] & Dmitri V. Talapin[1,4]

A colloidal solution is a homogeneous dispersion of particles or droplets of one phase (solute) in a second, typically liquid, phase (solvent). Colloids are ubiquitous in biological, chemical and technological processes[1,2], homogenizing highly dissimilar constituents. To stabilize a colloidal system against coalescence and aggregation, the surface of each solute particle is engineered to impose repulsive forces strong enough to overpower van der Waals attraction and keep the particles separated from each other[2]. Electrostatic stabilization[3,4] of charged solutes works well in solvents with high dielectric constants, such as water (dielectric constant of 80). In contrast, colloidal stabilization in solvents with low polarity, such as hexane (dielectric constant of about 2), can be achieved by decorating the surface of each particle of the solute with molecules (surfactants) containing flexible, brush-like chains[2,5]. Here we report a class of colloidal systems in which solute particles (including metals, semiconductors and magnetic materials) form stable colloids in various molten inorganic salts. The stability of such colloids cannot be explained by traditional electrostatic and steric mechanisms. Screening of many solute–solvent combinations shows that colloidal stability can be traced to the strength of chemical bonding at the solute–solvent interface. Theoretical analysis and molecular dynamics modelling suggest that a layer of surface-bound solvent ions produces long-ranged charge-density oscillations in the molten salt around solute particles, preventing their aggregation. Colloids composed of inorganic particles in inorganic melts offer opportunities for introducing colloidal techniques to solid-state science and engineering applications.

In this work, we synthesized various solutes—nanocrystals (NCs) of metals, semiconductors, rare-earth compounds and magnetic materials—using organic surfactants (for example, n-alkyl carboxylic acids) that stabilize colloidal solutions in non-polar solvents (Supplementary Methods). These organic surfactants are not compatible with molten inorganic salts, but they can be exchanged with inorganic surface ligands[6], which is expected to reduce the free energy of the interface between the NC surface and inorganic solvent. Moreover, surfactant-free (or 'bare') colloidal NCs can be prepared using ligand-stripping agents such as trimethyloxonium tetrafluoroborate[7] (see Methods). These recent developments in NC surface chemistry have been used to integrate NCs in inorganic hosts by co-precipitation from suitable solvents[8,9].

We studied the colloidal behaviour of different NCs in inorganic molten salts. For experimental convenience, we used salts with melting temperatures, T_m, below 350 °C. Such formulations can be prepared from metal halides, nitrates or thiocyanates (Extended Data Table 1). For example, a mixture containing $AlCl_3$, NaCl and KCl with a molar ratio $AlCl_3$:NaCl:KCl = 63.5:20:16.5 mol% (Extended Data Fig. 1a) has a T_m of ~90 °C, which is lower than the boiling points of many organic solvents. This molten salt can be interfaced with colloidal NCs dispersed in, for example, n-decane, which has a boiling point of 174 °C (Fig. 1a). After stirring for a short time, we observed a complete transfer of NCs from the n-decane phase to the molten salt (Fig. 1a and Extended Data Fig. 1b). The organic phase can be removed and NCs in molten salt can

be handled as ordinary colloidal solutions. Stable NC dispersions were also obtained after NC powders were mixed with molten salts and by other methods (see Methods). We prepared colloidal solutions of different metals (Pt, Pd), semiconductor quantum dots (such as InP NCs, and CdSe/CdZnS core/shell NCs, referred to as QDs), oxide (Fe_3O_4), and upconverting nanoparticles (UCNPs, such as $NaYF_4$:Yb,Er/CaF_2 core/shell NPs) (Fig. 1b and Extended Data Fig. 1c) in $AlCl_3$/NaCl/KCl molten salt. Similarly, we made colloidal NC solutions in other molten salts, including CsBr/LiBr/KBr ($T_m = 230$ °C), LiCl/LiBr/KBr ($T_m = 320$ °C), LiCl/LiI/KI ($T_m = 270$ °C), $AlBr_3$ ($T_m = 98$ °C), $ZnCl_2$/NaCl/KCl ($T_m = 203$ °C) and NaSCN/KSCN ($T_m \approx 130$–140 °C), as shown in Fig. 1c, d and Extended Data Fig. 1d. These examples demonstrate an impressive versatility of NC colloids in various molten salts (Extended Data Table 1). At the same time, not every combination of NCs and molten salts yielded stable colloids. For example, we were not able to make stable NC colloids in nitrate melts (for example, $LiNO_3$/$NaNO_3$/KNO_3/$CsNO_3$/$Ca(NO_3)_2$, $T_m \approx 65$ °C). This observation is in agreement with several prior works that discussed metastability of particle suspensions in the nitrate and carbonate melts[10].

Pt NCs dispersed in molten salt and Pt NC colloids in heptadecane or toluene showed very similar small angle X-ray scattering (SAXS) patterns typical of stable colloidal solutions (Fig. 2a). For comparison, a suspension of aggregated Pt NCs prepared by adding ethanol to a colloid of Pt NCs in toluene had a qualitatively different SAXS pattern with a pronounced peak at $q \approx 0.1$ Å^{-1} from NC aggregates[11]. We noticed no significant differences in the X-ray diffraction (XRD) patterns and transmission electron microscopy (TEM) images of original Pt NCs and the NCs recovered from the molten salt (Fig. 2b–e, Extended Data Fig. 2), suggesting that NC size and shape did not change after dispersion in molten salt. In contrast, significant differences were observed in the infrared (IR) absorption spectra of original and recovered NCs, which can be explained by the complete removal of organic ligands from the NC surface after transfer to molten salt (Extended Data Fig. 2d). CdSe/CdZnS QDs dispersed in NaSCN/KSCN molten salt showed bright photoluminescence (PL) when excited with UV light, while UCNPs in the same medium showed anti-Stokes emission when illuminated with a 980 nm near-infrared (IR) laser (Fig. 1e and Extended Data Fig. 3). Comparison of the emission spectra in traditional organic solvents and molten salts revealed no solvent-specific changes in the electronic structure or carrier dynamics of the QDs and UCNPs (Extended Data Fig. 3e, g–l). These structural, morphological and optical characteristics confirm the integrity of NCs dispersed in molten salts.

It appears that traditional stabilization mechanisms cannot explain the colloidal stability of NCs in a molten inorganic salt. The refractive index of NCs is generally higher than that of the molten salt (for example, $n \approx 2.5$ for CdSe compared with $n \approx 1.4$ for molten KCl) and van der Waals attraction cannot be eliminated by index matching. A very high charge density in a molten salt is expected to result in strong electrostatic screening, making Coulomb repulsive forces short-ranged and weaker than van der Waals attraction[12] (Supplementary Discussion). The absence of brush-like molecules tethered to the NC surface also rules out the possibility of classical steric colloidal stabilization[2].

[1]Department of Chemistry and James Franck Institute, University of Chicago, Chicago, Illinois 60637, USA. [2]Department of Biochemistry and Molecular Pharmacology, University of Massachusetts Medical School, Worcester, Massachusetts 01605, USA. [3]Advanced Photon Source, Argonne National Laboratory, Argonne, Illinois 60439, USA. [4]Center for Nanoscale Materials, Argonne National Laboratory, Argonne, Illinois 60439, USA.
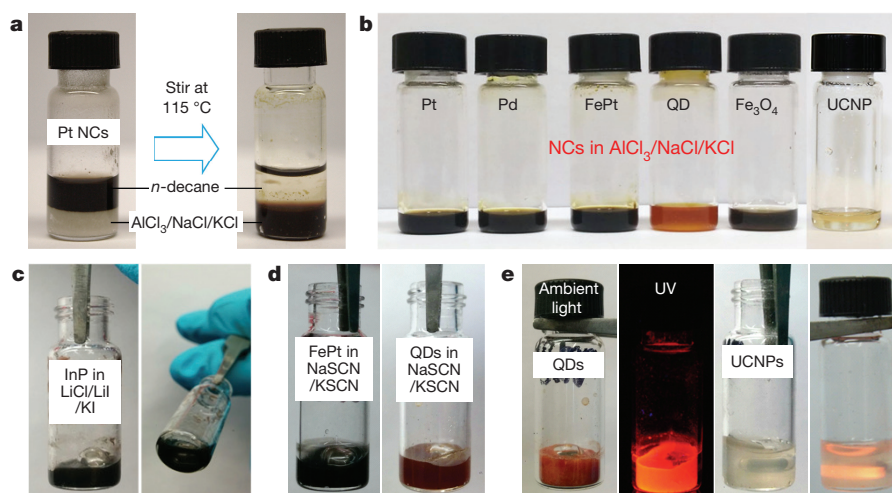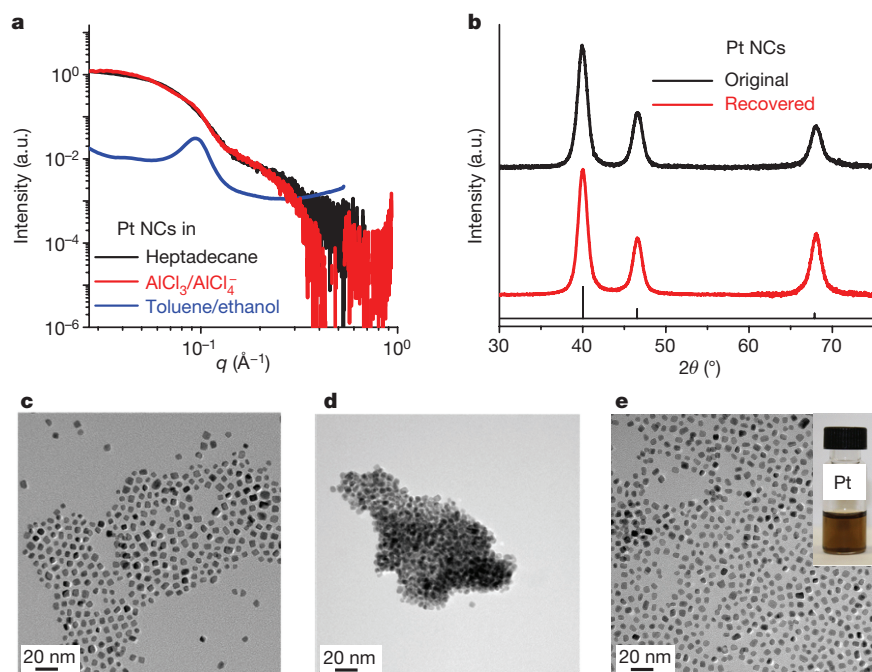
Figure 1 | Nanocrystal colloids in molten inorganic salts. a, Photographs of phase transfer of 5.5 nm Pt NCs from *n*-decane (upper liquid layer) to eutectic $AlCl_3/NaCl/KCl$ molten salt denoted in the text by $AlCl_3/AlCl_4^-$ (lower layer). **b–d**, Photographs of colloidal solutions of various NCs in molten inorganic salts; **b**, $AlCl_3/NaCl/KCl$ (~5 mg ml^{-1} for all NCs shown); **c**, LiCl/LiI/KI (~5 mg ml^{-1} for InP NCs viewed from two different angles), **d**, NaSCN/KSCN (~10 mg ml^{-1} for FePt, left, and for CdSe/CdZnS QDs, right). **e**, Photographs showing that CdSe/CdZnS QDs (left pair of images; ~10 mg ml^{-1}) and NaYF$_4$:Yb,Er/CaF$_2$ UCNPs (right pair; ~10 mg ml^{-1}) preserved their luminescence properties in molten NaSCN/KSCN when illuminated by a UV lamp or a 980 nm near-IR laser.

To understand the origin of colloidal stabilization in molten inorganic salts, we carried out a series of experimental and computational studies. We found a pattern relating colloidal stability and the chemical nature of NCs and molten salts: stable colloids formed only when there was a chemical affinity between the NC surface and ions present in the molten salt (Extended Data Table 1, Extended Data Fig. 4). This can be demonstrated using the family of $AlCl_3/NaCl/KCl$ molten salts. In melts that contain 50 mol% $AlCl_3$, $AlCl_3$ completely reacts with Cl^- ions and generates highly stable $[AlCl_4]^-$ ions[13]. The resulting NaAlCl$_4$/KAlCl$_4$ molten salt ($T_m = 123$ °C) does not contain components with pronounced Lewis acidity (for example, $AlCl_3$) or basicity (for example, Cl^-) and will be referred to as 'Lewis neutral'. In contrast, the salt formulations with more than 50 mol% $AlCl_3$ (for example, $AlCl_3$:NaCl:KCl = 63.5:20:16.5 mol%, further referred to as $AlCl_3/AlCl_4^-$) contain $[Al_2Cl_7]^-$ ions in equilibrium with aluminium chloride (in the form

of Al_2Cl_6 and $AlCl_3$)[13] and form molten salts with pronounced Lewis acidity. We found that Pt NCs formed stable colloids only in Lewis acidic melts containing excess $AlCl_3$ (that is, >50 mol% $AlCl_3$). When the Lewis neutral form of this molten salt was used, severe aggregation of NCs was observed (Fig. 3a). Similar behaviour was observed for Pd and other NCs shown in Fig. 1b in the Lewis neutral salts containing $[AlCl_4^-]$, $[AlBr_4^-]$ or NO_3^- ions (Extended Data Fig. 4). Electron-rich late transition metals (Pt^0, Pd^0) or chalcogenide (for example, Se^{2-} in CdSe) sites at the NC surface form chemical bonds to $AlCl_3$, behaving like σ-acceptor Z-type ligands as defined by Green's covalent bond classification. This type of bonding has been observed in molecular compounds, for example, in Pt(PCy$_3$)$_2$(AlCl$_3$) where Cy = cyclohexyl[14].

Mixed alkali metal salts with Lewis-basic halide (for example, LiCl/LiI/KI) and pseudohalide (for example, NaSCN/KSCN) ions also provided colloidal stability to various NCs (Fig. 1c, d). Since halide ions are relatively weak nucleophiles, removing the native organic coating using

Figure 2 | The nanocrystals stay intact in molten inorganic salts. a, SAXS intensity for Pt NC colloids in heptadecane, $AlCl_3/NaCl/KCl$ (denoted as $AlCl_3/AlCl_4^-$) eutectic molten salt, and a mixture of toluene and ethanol. **b**, Powder XRD patterns of original Pt NCs capped with a mixture of oleic acid (OA) and oleylamine (OLA), and bare NCs recovered from $AlCl_3/NaCl/KCl$ molten salt. The line pattern (bottom) shows the diffraction peaks for bulk fcc Pt phase. **c–e**, TEM images of Pt NCs with native OA and OLA ligands (**c**), bare NCs recovered from $AlCl_3/NaCl/KCl$ (**d**) and NCs recovered from $AlCl_3/NaCl/KCl$ and refunctionalized with OA and OLA ligands (**e**). Inset in **e**, photograph of a stable colloidal solution of recovered Pt NCs dispersed in toluene after organic ligands were added.
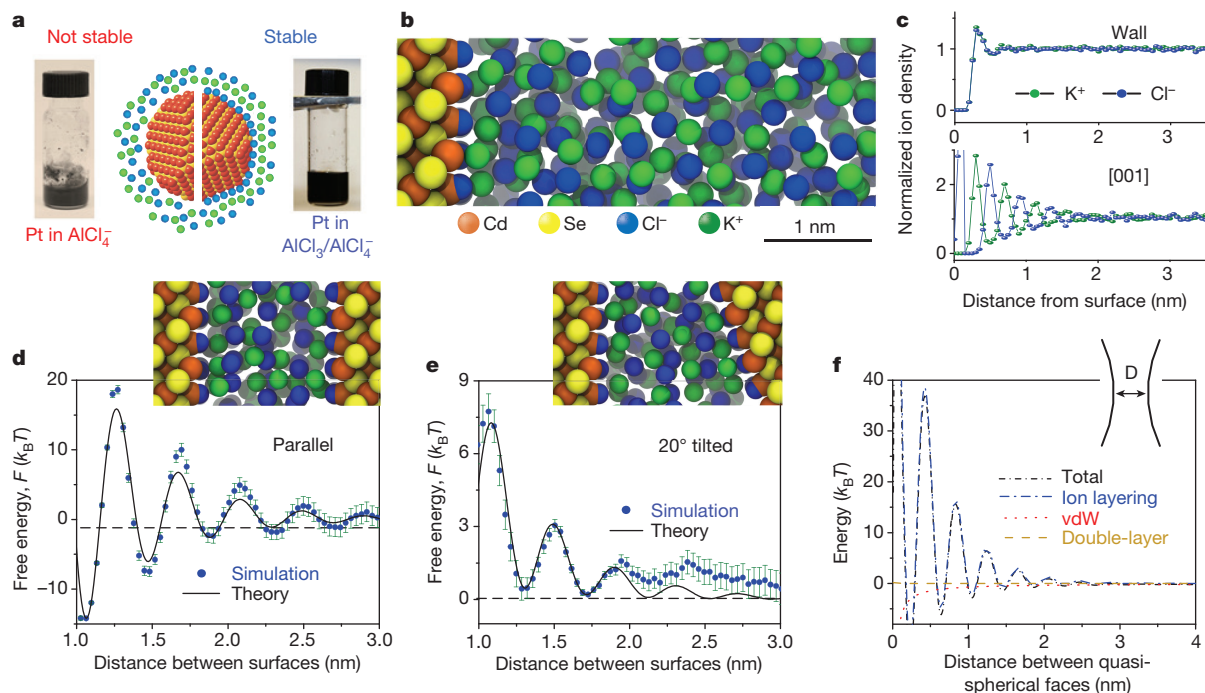
Figure 3 | The origin of colloidal stability in molten salts. a, Centre, relationship between colloidal stability and the chemical affinity of the NC surface (red) with species in the molten salt (represented by blue and green spheres). Corresponding examples of stable (right) and unstable (left) colloidal dispersions are shown in the photographs. **b**, A snapshot of MD simulation of the interface between the Cd-terminated [001] surface of a zinc-blende-structured CdSe crystal (left) and molten KCl (right). **c**, Density profiles of K^+ and Cl^- ions, showing the structuring of molten salt near the interface with a chemically inert wall (top) and with a Cd-terminated [001] (bottom) surface of zinc-blende CdSe crystal.

The crystal surface templates strong ordering of the molten salt. **d, e**, Simulated free energy of ion structuring in molten KCl (blue dots) between two [001] CdSe surfaces parallel to each other (**d**) and tilted by 20° (**e**). See the Methods subsection 'MD simulation and theoretical analysis of CdSe NC colloids in molten KCl' for details of error bars. Black lines are the predictions from continuum Ginzburg–Landau theory. **f**, Simulated free energy of the interactions between two spheroid NCs (diameter 10 nm); shown are total energy, and contributions from ion layer structuring, and from van der Waals (vdW) and electrostatic double-layer interactions.

ligand-stripping agents helped expose the undercoordinated electrophilic metal sites at the NC surface. Nucleophilic halide and pseudohalide anions interact with these sites as σ-donors (for example, Cl^- and SCN^- very efficiently bind to Cd^{2+} sites at CdSe NC surfaces[15,16]). The binding of SCN^- ions to QD surfaces was directly observed in IR absorption spectra (Extended Data Fig. 2e).

Inorganic nanoparticles form colloids in room temperature ionic liquids (ILs)[17–20], which are organic analogues of inorganic molten salts. Our studies of CdSe NCs in various ILs revealed two distinct mechanisms for the latter to support NC colloidal stability. First, stable colloids formed when the organic ligands on NCs could be efficiently solvated by the IL, as in the case of oleate-capped CdSe NCs dispersed in highly hydrophobic trihexyl(tetradecyl)phosphonium bis(2,4,4-trimethylpentylphosphinate) IL. NCs dispersed in such ILs preserved their original organic ligand shells (Extended Data Fig. 5 and Supplementary Discussion). The steric repulsion of organic ligands can explain the stability of many reported NC colloids in ILs. Second, we also observed stable colloids in hydrophilic ILs that could not efficiently solvate NC ligands, but contained ions with sufficient nucleophilicity and affinity for the NC surface (for example, Cl^- in 1-butyl-3-methylimidazolium chloride, $[BMIM]^+Cl^-$). CdSe NCs formed stable colloids in $[BMIM]^+Cl^-$ after the original organic ligands were displaced from the NC surface by Cl^- ions (Extended Data Fig. 5 and Supplementary Discussion). No colloidal stabilization occurred if ILs lacked anions with strong surface binding affinity (for example, $[BMIM]^+BF_4^-$, Extended Data Fig. 6a). Such behaviour of NCs in ILs corroborates the observations for NCs in molten inorganic salts. However, it should be noted that several recent studies reported very large, up to ~10 nm, Debye screening lengths measured in pure organic ILs[21,22] and explained by the low degree of dissociation of ILs, which points to a qualitative difference in ionic equilibria between room temperature organic ILs and molten inorganic salts[21].

To gain further insights into the origin of colloidal stability, we modelled the interface between the CdSe crystal and molten KCl using molecular dynamics (MD) simulations (Fig. 3b and Supplementary Discussion). Solvent structuring takes place near every solid–liquid interface, regardless of the interaction between the surface and solvent[2]; it typically creates decaying solvent density oscillations that propagate for several molecular diameters[23]. Ion layering near interfaces has been reported in molten salts and organic ILs[24], and it was also observed in our simulations. Near the interface with a chemically inert hard wall, both K^+ and Cl^- ions showed identical oscillatory density profiles that decayed to the bulk density within less than 0.5 nm (Fig. 3c, top panel). In contrast, cadmium-terminated [001] and [111] CdSe surfaces, which are the typical facets of zinc-blende-structure CdSe NCs[25], induced a qualitatively different behaviour in the molten salt. In agreement with previous experimental data[15], CdSe NCs showed a strong affinity towards Cl^- ions that formed a dense, nearly epitaxial surface layer (see Supplementary Discussion). These co-ions templated strong ordering in the molten salt, with alternating K^+ and Cl^- shells extending into the liquid phase for about 2 nm (Fig. 3b and bottom panel in Fig. 3c). The ion shells created charge density oscillations around each NC, which were robust with respect to temperature above T_m (Extended Data Fig. 7a, b).

When two NCs approach each other to a distance smaller than twice the length of the structured ion layers, the interference between charge density oscillations contributes to attraction or repulsion of the NC cores. To evaluate the free energy of this interaction, we carried out umbrella sampling simulations (Supplementary Discussion). For two parallel surfaces, the surface-templated charge density oscillations can interfere constructively or destructively, depending on the distance, which leads to an exponentially decaying oscillatory interaction energy (Fig. 3d). However, any tilt between the two surfaces causes

suppression of the oscillatory component and development of a repulsive force between the approaching surfaces owing to frustration of the molten salt layers (Fig. 3e). The interaction energy between two 10-nm spheroid NCs was calculated by modelling each spheroid as a linear combination of differently tilted plates (Fig. 3f, Extended Data Fig. 7c and Supplementary Discussion). This repulsive-oscillatory force of ion structuring by far exceeds both the van der Waals and the double-layer electrostatic contributions at all interparticle separations, except at very short, subnanometre distances (Fig. 3f), and the ionic structure near NC interface is responsible for the colloidal stability.

To rationalize these MD simulations, we applied a phenomenological Ginsburg–Landau theory to solvation in molten salts. Using the Derjaguin approximation, the interaction energy of ion structuring between spherical particles, V, can be derived as $V(D) \approx \pi R l_c e^{-D/l_c}(\cos(q_0 D) + l_c/R)$, where D is the distance between the approaching surfaces, R is the particle radius, q_0 is the wavenumber for charge density oscillations and l_c is the correlation length (see Supplementary Discussion). Our theory shows very good agreement with MD simulations, as seen in Fig. 3d, e, and further supports the important role of ion structuring near curved surfaces for colloidal stabilization of NCs in molten salts. In the absence of surface-templated charge density oscillations, the force between NCs was predicted to be solely attractive by the theoretical analysis, and this was also observed in simulations (Extended Data Fig. 7d), in agreement with the experimental data. The oscillatory-repulsive forces between NCs in molten salts bear a similarity to the hydration repulsion between polar surfaces in water[26,27], although the physical origin of these forces appears to be different.

Our preliminary studies suggest that the range of unconventional inorganic solvents can be extended beyond molten inorganic salts. For example, Pt NCs can be surface-engineered to form dispersions in liquid metals, such as the Ga–In eutectic and Wood's metal (a Bi-Pb-Sn-Cd alloy; Extended Data Fig. 8). We note that infusing metals with nanoparticles can markedly enhance their strength, stiffness and durability[28], and that integration of semiconductor and oxide NCs into inorganic hosts by co-precipitation from suitable solvents has been useful in several energy-related applications[8,9]. Also, with their ability to form stable colloidal solutions, size- and shape-tailored particles could be employed to increase the thermal conductivity of molten salts used for heat transfer and thermal storage[29,30]. Finally, molten salts and liquid metals can be used as media for colloidal synthesis of new nanomaterials (Extended Data Fig. 9).

Online Content Methods, along with any additional Extended Data display items and Source Data, are available in the online version of the paper; references unique to these sections appear only in the online paper.

1. Evans, D. F. & Wennerström, H. *The Colloidal Domain: Where Physics, Chemistry, Biology and Technology Meet* 1–503 (Wiley-VCH, 1999).
2. Israelachvili, J. N. *Intermolecular and Surface Forces* 3rd edn 1–674 (Elsevier Academic, 2011).
3. Derjagin, B. V. & Landau, L. Theory of the stability of strongly charged lyophobic sols and of the adhesion of strongly charged particles in solution of electrolytes. *Acta Physicochim. URSS* **14,** 633–662 (1941).
4. Verwey, E. J. W. & Overbeek, J. T. G. *Theory of the Stability of Lyophobic Colloids* 1–205 (Elsevier, 1948).
5. Napper, D. H. Steric stabilization. *J. Colloid Interface Sci.* **58,** 390–407 (1977).
6. Kovalenko, M. V., Scheele, M. & Talapin, D. V. Colloidal nanocrystals with molecular metal chalcogenide surface ligands. *Science* **324,** 1417–1420 (2009).
7. Rosen, E. L. *et al.* Exceptionally mild reactive stripping of native ligands from nanocrystal surfaces by using Meerwein's salt. *Angew. Chem. Int. Ed.* **51,** 684–689 (2012).
8. Ning, Z. *et al.* Quantum-dot-in-perovskite solids. *Nature* **523,** 324–328 (2015).
9. Boles, M. A., Ling, D., Hyeon, T. & Talapin, D. V. The surface science of nanocrystals. *Nat. Mater.* **15,** 141–153 (2016).
10. Andreu-Cabedo, P. *et al.* Increment of specific heat capacity of solar salt with SiO₂ nanoparticles. *Nanoscale Res. Lett.* **9,** 582–592 (2014).
11. Murray, C. B., Kagan, C. R. & Bawendi, M. G. Synthesis and characterization of monodisperse nanocrystals and close-packed nanocrystal assemblies. *Annu. Rev. Mater. Sci.* **30,** 545–610 (2000).
12. Lanning, O. J. & Madden, P. A. Screening at a charged surface by a molten salt. *J. Phys. Chem. B* **108,** 11069–11072 (2004).
13. Fannin, A. A. Jr, King, L. A. & Seegmiller, D. W. Chloroaluminate equilibria in AlCl₃–NaCl melts. *J. Electrochem. Soc.* **119,** 801–807 (1972).
14. Amgoune, A. & Bourissou, D. σ-Acceptor, Z-type ligands for transition metals. *Chem. Commun.* **47,** 859–871 (2011).
15. Zhang, H., Jang, J., Liu, W. & Talapin, D. V. Colloidal nanocrystals with inorganic halide, pseudohalide, and halometallate ligands. *ACS Nano* **8,** 7359–7369 (2014).
16. Fafarman, A. T. *et al.* Thiocyanate-capped nanocrystal colloids: vibrational reporter of surface chemistry and solution-based route to enhanced coupling in nanocrystal solids. *J. Am. Chem. Soc.* **133,** 15753–15761 (2011).
17. Warren, S. C. *et al.* Generalized route to metal nanoparticles with liquid behavior. *J. Am. Chem. Soc.* **128,** 12074–12075 (2006).
18. Gao, J., Ndong, R. S., Shiflett, M. B. & Wagner, N. J. Creating nanoparticle stability in ionic liquid [C₄mim][BF₄] by inducing solvation layering. *ACS Nano* **9,** 3243–3253 (2015).
19. Ueno, K., Inaba, A., Kondoh, M. & Watanabe, M. Colloidal stability of bare and polymer-grafted silica nanoparticles in ionic liquids. *Langmuir* **24,** 5253–5259 (2008).
20. Rodriguez, R., Herrera, R., Archer, L. A. & Giannelis, E. P. Nanoscale ionic materials. *Adv. Mater.* **20,** 4353–4358 (2008).
21. Gebbie, M. A., Dobbs, H. A., Valtiner, M. & Israelachvili, J. N. Long-range electrostatic screening in ionic liquids. *Proc. Natl Acad. Sci. USA* **112,** 7432–7437 (2015).
22. Smith, A. M., Lee, A. A. & Perkin, S. The electrostatic screening length in concentrated electrolytes increases with concentration. *J. Phys. Chem. Lett.* **7,** 2157–2163 (2016).
23. Zobel, M., Neder, R. B. & Kimber, S. A. J. Universal solvent restructuring induced by colloidal nanoparticles. *Science* **347,** 292–294 (2015).
24. Mezger, M. *et al.* Molecular layering of fluorinated ionic liquids at a charged sapphire (0001) surface. *Science* **322,** 424–428 (2008).
25. Erwin, S. C. *et al.* Doping semiconductor nanocrystals. *Nature* **436,** 91–94 (2005).
26. Israelachvili, J. N. & Wennerström, H. Role of hydration and water structure in biological and colloidal interactions. *Nature* **379,** 219–225 (1996).
27. Schneck, E., Sedlmeier, F. & Netz, R. R. Hydration repulsion between biomembranes results from an interplay of dehydration and depolarization. *Proc. Natl Acad. Sci. USA* **109,** 14405–14409 (2012).
28. Chen, L.-Y. *et al.* Processing and properties of magnesium containing a dense uniform dispersion of nanoparticles. *Nature* **528,** 539–543 (2015).
29. Li, C.-J., Li, P., Wang, K. & Molina, E. E. Survey of properties of key single and mixture halide salts for potential application as high temperature heat transfer fluids for concentrated solar thermal power systems. *AIMS Energy* **2,** 133–157 (2014).
30. Özerinç, S., Kakaç, S. & Yazıcıoğlu, A. Enhanced thermal conductivity of nanofluids: a state-of-the-art review. *Microfluid. Nanofluidics* **8,** 145–170 (2010).

Author Contributions H.Z. performed and designed the experiments, analysed data, and co-wrote the paper. G.H. provided UCNPs. B.L. set up SAXS measurements and analysed data. K.D., N.B.L. and S.V. designed and carried out theoretical analysis and MD simulations. D.V.T. conceived and designed experiments and simulations, analysed data, co-wrote the paper, and supervised the project. All authors discussed the results and commented on the manuscript.

Author Information Reprints and permissions information is available at www.nature.com/reprints. The authors declare no competing financial interests. Readers are welcome to comment on the online version of the paper. Correspondence and requests for materials should be addressed to D.V.T. (dvtalapin@uchicago.edu).

METHODS

Nanocrystal syntheses. We synthesized nanocrystals (NCs) according to reported methods using conventional air-free techniques. Details are provided in the Supplementary Methods.

Ligand removal of nanocrystals. To facilitate the dispersion of NCs in molten inorganic salts and liquid metals, the native organic surface ligands of NCs were removed with ligand-stripping agents. For instance, 2 ml of an FePt (or upconverting nanoparticles (UCNPs), Fe_3O_4, Pt, Pd) NC dispersion in hexane (5 mg ml^{-1}) was mixed with 2 ml of 0.01 M nitrosonium tetrafluoroborate (NOBF$_4$, 97%, Aldrich) solution in dichloromethane[31]. The mixture was vigorously stirred until the NCs precipitated, typically within 30 min. The UCNPs needed to be stirred for a longer period of time (up to 10 h). The bare NCs were separated from the supernatant by centrifugation and dispersed well in N,N-dimethylformamide (DMF). To purify these NCs, a mixture of toluene/hexane (1:1 by volume) was added as a non-solvent to flocculate NCs, which were then redispersed in fresh DMF. The purification process was repeated 2 or 3 times. Removing native ligands from InP and CdSe NCs (or CdSe/CdZnS core/shell quantum dots (QDs)) was achieved by using tetrafluoroboric acid (HBF$_4$, 50–55% w/w with diethyl ether, Alfa Aesar)[32] and trimetyloxonium tetrafluoroborate (Me$_3$OBF$_4$, 95%, Aldrich)[7] as ligand-stripping agents, respectively.

Dispersion and recovery of nanocrystals in molten inorganic salts. All procedures were performed in a glove box filled with N$_2$ unless otherwise stated. Caution: to disperse NCs, inorganic salts were typically heated to 100–300 °C to a molten state. Vials containing molten inorganic salts need to be handled with care. NCs can disperse in molten inorganic salts in several ways. First, Pt NCs can disperse in a ternary mixture with a composition of AlCl$_3$:NaCl:KCl = 63.5:20:1 6.5 mol% (further referred to as AlCl$_3$/AlCl$_4^-$) through a phase transfer process. In this procedure, a solution of Pt NCs in decane (about 0.3 ml, 5 mg ml^{-1}) was combined with molten AlCl$_3$/AlCl$_4^-$ (about 0.3 ml). The resulting mixture was stirred with a Pyrex-glass-coated stir bar until NCs completely transferred from the upper, organic phase to the molten salt solvent, typically within 15 min. Pt NC colloids in AlCl$_3$/AlCl$_4^-$ can also be achieved using a solvent-free method. In this approach, dried NC solids were mixed with solidified AlCl$_3$/AlCl$_4^-$, then heated to about 120 °C, and stirred. A homogeneous Pt NC colloid was typically obtained within 30 min. A third procedure involved adding a small volume of NC dispersion in hexane into molten AlCl$_3$/AlCl$_4^-$. For instance, a small drop (0.025 ml) of hexane containing 1–5 mg of Pt NCs was quickly added to 0.6 g (about 0.4 ml) of molten AlCl$_3$/AlCl$_4^-$. The hexane vaporized upon contact because of the high temperature. The Pt NCs formed a stable, black colloid in AlCl$_3$/AlCl$_4^-$ while being stirred. Using the above approaches, various NCs (for example, Pd, FePt, UCNPs) with coordinated organic ligands, naked surfaces, or inorganic ligands (the last two typically with the solvent-free method) can form stable colloids in AlCl$_3$/AlCl$_4^-$. An Fe$_3$O$_4$ NC colloid in AlCl$_3$/AlCl$_4^-$ was obtained from dried bare NCs using the solvent-free method. Depending on a number of factors, including the type and concentration of NCs and dispersion methods, it may take less than 5 min to hours for stable NC colloids to form.

Stable NC colloids in halide-based (for example, LiCl/LiI/KI) or pseudohalide-based (for example, NaSCN/KSCN) molten salts were obtained from bare NCs/molten salts mainly using the solvent-free method. For instance, about 5 mg of dried, bare UCNPs were mixed with 0.5 g of NaSCN/KSCN (about 0.3 ml in the molten state at about 130 °C) at room temperature. The resulting mixture was stirred at 130 °C for several hours until UCNPs formed a homogeneous, stable colloid in the molten salt. A similar procedure can be applied to other bare NCs. It typically takes several hours to a day to disperse the NC solids in salts, depending on the combinations of NCs and salts, the amount of NCs, and the stirring conditions.

For further morphological, structural, surface and compositional characterizations, NCs were recovered from molten salts after the salt matrices were dissolved with a single solvent or a series of solvents, depending on the compositions of salts. To recover NCs from AlCl$_3$/AlCl$_4^-$, a sequential washing procedure with a large excess of anhydrous diethyl ether and tetrahydrofuran (THF) was performed in a glove box filled with N$_2$. These aprotic solvents can dissolve the Lewis acidic components ([Al$_2$Cl$_7^-$] with minor Al$_2$Cl$_6$, AlCl$_3$) by forming Lewis acid–base complexes. (We note that any residual moisture or protic solvents may react with [Al$_2$Cl$_7^-$], forming acidic species that may damage NCs). The residual salts were dissolved in methanol and water, in air. NCs were collected by centrifugation, washed with water, and dried before characterizations. Similarly, NCs can be recovered from NaSCN/KSCN (acetone or water), LiCl/LiI/KI (anhydrous methanol, followed by water), and other salt matrices.

In some cases, the recovered NC solids can be functionalized using additional organic ligands and redispersed in non-polar solvents (toluene or hexane) through sonication. For instance, 5 mg of dried Pt NCs (or Pd, Fe$_3$O$_4$ NCs, and UCNPs) recovered from AlCl$_3$/AlCl$_4^-$ can form a stable solution in 1 ml of toluene with 0.1–0.2 ml of OA and OLA after being sonicated for about 30 min. A conventional purification process using toluene/ethanol as a solvent/non-solvent pair was applied to remove excess organic ligands. Finally, NCs functionalized with organic ligands were dispersed in toluene or hexane.

Dispersion and recovery of nanocrystals in ionic liquids. NCs (such as CdSe, Pt, Fe$_3$O$_4$, FePt, QDs) functionalized by organic ligands in toluene were dried under vacuum to remove organic solvents. The dried NCs were mixed with hydrophobic ionic liquids (ILs), such as trihexyl(tetradecyl)phosphonium bis(2,4,4-trimethylpentyl) phosphinate (P$^+$P$^-$), in a glove box filled with N$_2$. After stirring for less than 30 min, we obtained a stable NC solution in P$^+$P$^-$ with a high concentration (>50 mg ml^{-1}). NC dispersions in P$^+$P$^-$ can be diluted with common non-polar solvents such as toluene without affecting colloidal stability. Adding acetonitrile or ethanol to NC dispersions in P$^+$P$^-$/toluene resulted in a flocculated solution. After centrifugation, NCs were recovered and redispersed in toluene, leaving P$^+$P$^-$ in the supernatant.

A phase transfer process was employed to disperse NCs in hydrophilic, imidazolium-based ILs, including [BMIM]$^+$Cl$^-$ and [BMIM]$^+$I$^-$, in a glove box filled with N$_2$. In brief, 1.0 ml of CdSe NCs with oleic acid/trioctylphosphine/trioctylphosphine oxide (OA/TOP/TOPO) in octane (15 mg ml^{-1}) was mixed with 1.0 g of [BMIM]$^+$Cl$^-$ (about 0.95 ml at 80 °C). Once the solution was vigorously stirred at 80 °C (the melting point of [BMIM]$^+$Cl$^-$ is 73 °C), the NCs gradually transferred to the bottom IL phase within several hours, resulting in a colourless top phase. The red-coloured [BMIM]$^+$Cl$^-$ phase was rinsed with fresh octane several times to remove residual organic ligands. Afterward, the slightly turbid IL phase was rinsed with anhydrous ethyl acetate multiple times to break the emulsions presumably from residual species related to organic ligands, resulting in a stable CdSe NC colloid in [BMIM]$^+$Cl$^-$. These NC colloids in [BMIM]$^+$Cl$^-$ are stable under inert atmosphere for several months. CdSe NCs in [BMIM]$^+$Cl$^-$ can be recovered by adding acetonitrile and separated from the supernatant, which contains acetonitrile and [BMIM]$^+$Cl$^-$. The recovered CdSe NCs can be redispersed in fresh [BMIM]$^+$Cl$^-$ to form a stable colloid once gently heated and stirred. In addition, CdSe NCs/[BMIM]$^+$Cl$^-$ remained colloidally stable after they were diluted with polar organic solvents such as N-methylformamide (NMF). NCs can also be recovered by adding H$_2$O to the solution in NMF, followed by centrifugation.

Phase transfer of CdSe NCs from octane to ILs was also observed when [BMIM]$^+$I$^-$ was used as the bottom phase. Similar purification processes were applied to achieve stable CdSe NC colloids in [BMIM]$^+$I$^-$ or to recover NCs. In the cases of [BMIM]$^+$BF$_4^-$, 1-ethyl-3-methylimidazolium ethylsulfate ([EMIM]$^+$[EtSO$_4$]$^-$), or 1-butyl-3-methylimidazolium octylsulfate ([BMIM]$^+$[OctSO$_4$]$^-$), no phase transfer was observed. However, CdSe NCs can be stabilized in [BMIM]$^+$BF$_4^-$ or [EMIM]$^+$[EtSO$_4$]$^-$ in the presence of a small amount of [BMIM]$^+$Cl$^-$ or [BMIM]$^+$I$^-$. For instance, CdSe NCs in 0.05–1 g of [BMIM]$^+$Cl$^-$ maintained colloidal stability after being diluted with 1.0 ml of [EMIM]$^+$[EtSO$_4$]$^-$.

Dispersion and recovery of nanocrystals in liquid metals. 2 ml of a bare Pt NC dispersion (1–5 mg ml^{-1}) in DMF was stirred in the presence of a droplet of liquid metal (about 0.5 g of Ga–In or Wood's alloy) at ~40 and 80 °C, respectively, for 1–3 days. Typically, the bare Pt NCs in DMF were destabilized while the mixture (Pt NCs in DMF with liquid metals) was stirred. Afterward, the mixture was allowed to cool to room temperature. The metal drop/slug was carefully separated from the supernatant and the insoluble NC precipitates, and was then washed with fresh DMF to remove NC residue on the metal surface. For Wood's alloy, the solidified metal slugs were gently polished with fine sand paper to completely remove the insoluble NC residue on the surface.

Pt NCs can be recovered with acid to digest the metal matrices. Ga–In was digested with diluted HCl (≥37%, TraceSELECT, for trace analysis, fuming, Aldrich); Wood's alloy or Sn–Pb alloy was digested by a mixture of HNO$_3$ (≥69%, TraceSELECT, for trace analysis, Aldrich) and HF (48 wt% in water, ≥99.99%, metal traces, Aldrich) diluted by deionized (DI) water. The samples in acids were sonicated to accelerate the digestion of metal matrices. Pt NCs were separated from the acidic solution by centrifugation and then rinsed with DI water.

MD simulation and theoretical analysis of CdSe NC colloids in molten KCl. To study the origin of colloidal stability in molten inorganic salts, we performed classical molecular dynamics (MD) and umbrella sampling simulations[33] of passivated CdSe NCs (in zinc-blende configuration) solvated in molten KCl salt. MD visualization was created using VMD software[34] and the error bars in MD simulation were related to state-state covariance as discussed elsewhere[35]. Detailed information on simulation methods and theoretical analysis[36] is available in the Supplementary Materials.

Characterization techniques. Transmission electron microscopy (TEM) of recovered NCs from molten inorganic salts or liquid metals were collected using a 300 kV FEI Tecnai F30 microscope. The recovered NC solids were suspended

in hexane and drop-cast on a carbon-coated copper grid. The TEM images of refunctionalized Pt or Fe_3O_4 NCs were prepared by drop-casting NC dispersion in toluene on TEM grids.

The structural information of recovered NCs was assessed from wide-angle powder X-ray diffraction (XRD) patterns using a Bruker D8 diffractometer with a Cu K_α X-ray source operating at 40 kV and 40 mA. In order to study the colloidal stability of NCs in molten inorganic salts and ILs, small angle X-ray scattering (SAXS) measurements were carried out at the 12-ID-B beamline (Advanced Photon Source, Argonne National Laboratory). A 14 keV X-ray beam was focused on samples with a $300 \times 20\,\mu m^2$ (H×V) beam size. A Pilatus2M detector for SAXS imaging was located about 2 m downstream of the samples. NCs in various media were prepared with a concentration of about 5 mg ml^{-1} in glass capillaries (0.3–0.8 mm), which were sealed using a flame or epoxy under inert atmosphere. The capillaries were then loaded to a THMS 600 Linkam hot stage for SAXS measurements at elevated temperatures. Samples in inorganic salts or IL matrices were heated to a molten state for SAXS measurements. For comparison, NC solutions/suspensions in toluene, heptadecane, and a mixture of toluene/ethanol with similar concentrations were also measured. The NC solution in heptadecane was measured at the same temperature with NC colloids in AlCl₃/AlCl₄⁻. The low signal-to-noise ratio in SAXS data at high q values in molten salts is related to high X-ray absorption by the molten salt as compared to traditionally used hydrocarbon solvents. At higher q values, the solvent background becomes comparable to the scattering signal from the nanoparticles.

The UV–visible spectra of CdSe NCs in toluene, P⁺P⁻, [BMIM]⁺I⁻, and mixed solvents were collected using a Cary 5000 ultraviolet-visible-near infrared (UV-Vis-NIR) spectrophotometer. Fourier transform infrared (FTIR) spectra of Pt NCs recovered from AlCl₃/AlCl₄⁻, QDs recovered from NaSCN/KSCN, and CdSe NCs recovered from P⁺P⁻ and [BMIM]⁺Cl⁻ or [BMIM]⁺I⁻ were acquired in transmission mode using a NicoletNexus-670 FTIR spectrometer. For quantitative comparison, the same amount of dried, organically capped, or recovered NC solids were mixed with KBr powder and pressed into pellets with the same dimensions. For qualitative analysis, photoluminescence (PL) spectra of QDs and UCNPs in organic solvents and NaSCN/KSCN (in both the molten and solidified states) were recorded using an optical fibre (Ocean Optics, QE Pro, QP600-1-UV-VIS) connected to an optical microscope (Olympus BX51). QDs and UCNPs were excited by a blue light (white light with a short-pass filter, cut-off at 492 nm) and a 980 nm IR laser, respectively. To monitor the PL spectra of NCs in molten NaSCN/KSCN, the samples were preheated at 150 °C. To quantitatively compare absorption features and PL intensities of QDs with native organic ligands, those recovered from NaSCN/KSCN, and those redispersed in toluene with the addition of organic ligands, the absorption and emission spectra of the QD solutions were collected using a Cary 5000 UV-Vis-NIR spectrophotometer and Nanolog fluorometer (Horiba JY), respectively.

¹H-NMR spectra of CdSe NC colloids in toluene and P⁺P⁻/toluene were recorded at 500 MHz on a Bruker Ultrashield 500 plus spectrometer. OA/TOP/TOPO-capped CdSe NCs in hexane were thoroughly dried and redispersed in 1.0 ml of d⁸-toluene with a concentration of 25 mg ml^{-1}. To probe the OA ligands on the surface of CdSe NCs in P⁺P⁻, 0.1 ml of CdSe/P⁺P⁻ (25 mg ml^{-1}) was diluted with 1.0 ml of d⁸-toluene. To test the presence of OA ligands on the surface of CdSe NCs in [BMIM]⁺Cl⁻, we recovered the original organic ligands by digesting CdSe NCs. In brief, DI water was added to CdSe NCs/[BMIM]⁺Cl⁻ (1.0 ml, 25 mg ml^{-1}) to cause the CdSe NCs to precipitate out while dissolving the IL matrix. The NC precipitates were rinsed several times with DI water to completely remove [BMIM]⁺Cl⁻. Afterward, NCs were digested in half-concentrated aqua regia following the standard procedure[6]. The organic ligands (OA/TOP/TOPO), if any, were then extracted with diethyl ether, dried under vacuum, and dissolved in d⁸-toluene (1.0 ml) for NMR study. All samples were measured at 298 K.

Inductively coupled plasma optical emission spectroscopy (ICP–OES) analysis of samples digested in acidic aqueous solutions was carried out on a Agilent 700 Series spectrometer. To probe the TOP and TOPO ligands on the surface of CdSe NCs in toluene, P⁺P⁻, and [BMIM]⁺Cl⁻, the same amount of NCs recovered from various solvents were digested by piranha solution and diluted with DI water. To prove the homogeneity of NCs in liquid metal, several aliquots of Pt NCs in Ga–In eutectic were digested by aqua regia and diluted with DI water for quantitative ICP–OES analysis of the ratio of Pt:Ga and Pt:In. Similarly, a piece of Wood's alloy (about 0.45 g) containing bare Pt NCs was digested by aqua regia, and diluted with DI water to determine the concentration of Pt NCs.

Sample size. No statistical methods were used to predetermine sample size.

Code availability. The simulations described in the paper were performed with publicly available simulation packages (LAMMPS). The scripts used for data analysis are available from S.V. (svaikunt@uchicago.edu) on request.

**Data availability.** The data supporting the findings of this study are available from D.V.T. on request.

31. Dong, A. *et al.* A generalized ligand-exchange strategy enabling sequential surface functionalization of colloidal nanocrystals. *J. Am. Chem. Soc.* **133,** 998–1006 (2011).
32. Huang, J. *et al.* Surface functionalization of semiconductor and oxide nanocrystals with small inorganic oxoanions (PO_4^{3-}, MoO_4^{2-}) and polyoxometalate ligands. *ACS Nano* **8,** 9388–9402 (2014).
33. Frenkel, D. & Smit, B. *Understanding Molecular Simulation* 2nd edn 165–199 (Elsevier Academic, 2002).
34. Humphrey, W., Dalke, A. & Schulten, K. VMD – Visual molecular dynamics. *J. Mol. Graph.* **14,** 33–38 (1996).
35. Shirts, M. R. & Chodera, J. D. Statistically optimal analysis of samples from multiple equilibrium states. *J. Chem. Phys.* **129,** 124105 (2008).
36. Limmer, D. T. Interfacial ordering and accompanying divergent capacitance at ionic liquid-metal interfaces. *Phys. Rev. Lett.* **115,** 256102 (2015).
37. Kohn, H. W. & Willmarth, T. E. Metallic colloids in molten salts. *Science* **163,** 924–925 (1969).
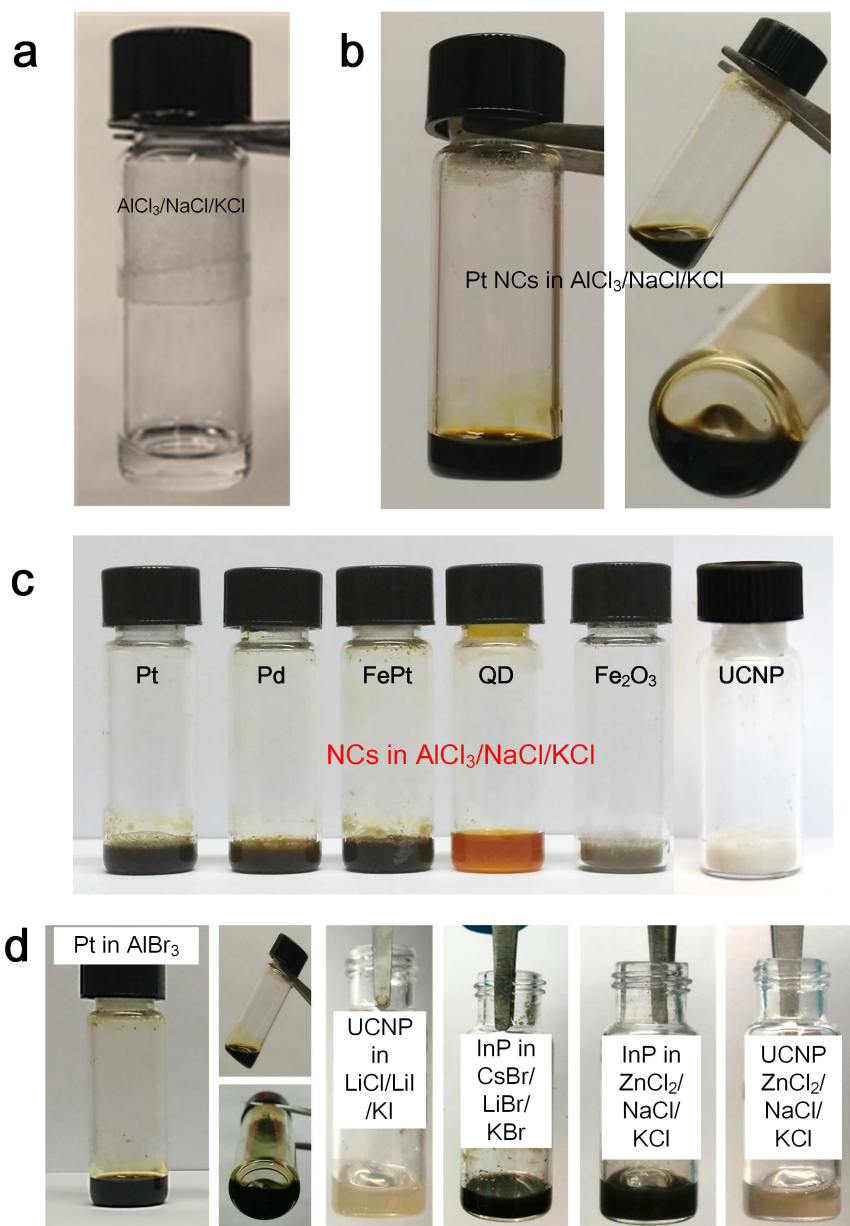
Extended Data Figure 1 | Photographs illustrating the generality of NC colloids in molten inorganic salts. a, The eutectic $AlCl_3/NaCl/KCl$ molten salt. **b**, A stable colloid ($\sim5\,mg\,ml^{-1}$) of Pt NCs in molten $AlCl_3/NaCl/KCl$ ($AlCl_3:NaCl:KCl = 63.5:20:16.5\,mol\%$, also referred to as $AlCl_3/AlCl_4^-$). The three photographs show the same colloid at different angles. **c**, Solidified samples of various NCs (labelled) in $AlCl_3/NaCl/KCl$ ($\sim5\,mg\,ml^{-1}$ for all NCs). **d**, Additional examples of various combinations of NCs and molten salts, including Pt NCs in molten $AlBr_3$, $NaYF_4$:Yb,Er/CaF_2 upconverting nanoparticles (UCNPs) in molten LiCl/LiI/KI, InP NCs in molten CsBr/LiBr/KBr, InP NCs in molten $ZnCl_2/NaCl/KCl$, and UCNPs in molten $ZnCl_2/NaCl/KCl$. The concentrations of NC dispersions shown in **d** are 5–$10\,mg\,ml^{-1}$.
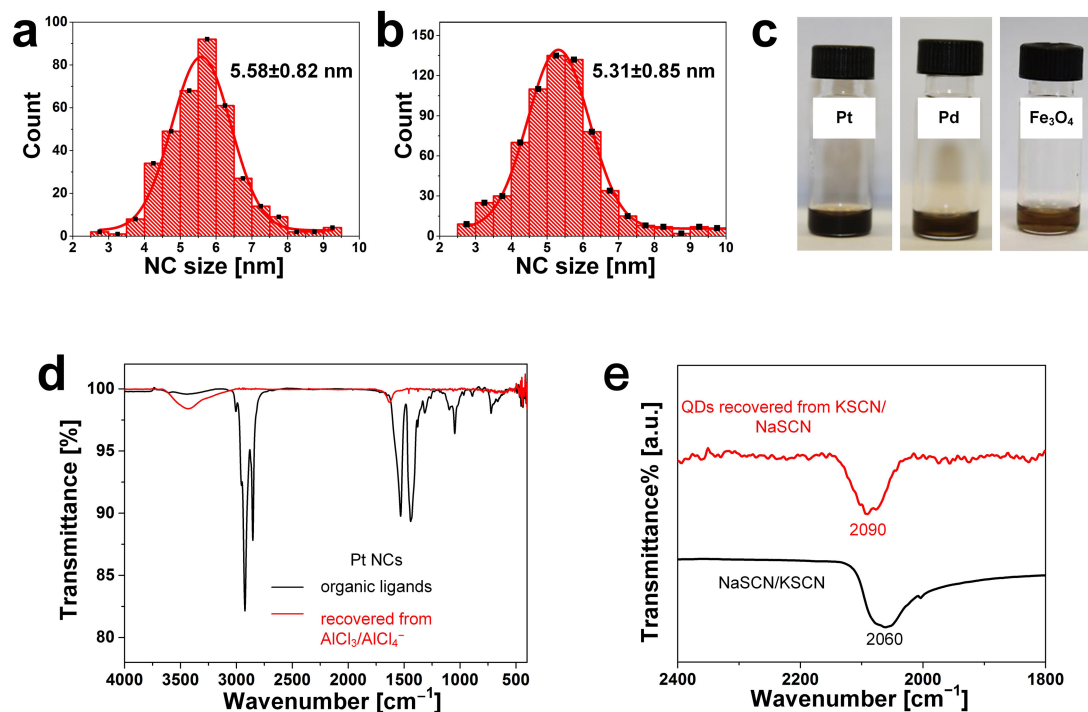
Extended Data Figure 2 | Integrity and surface chemistry of NCs in molten salts. a, **b**, Histograms of the size distributions of Pt NCs: **a**, with native OA and OLA ligands, and **b**, NCs recovered from $AlCl_3/NaCl/KCl$ and refunctionalized with OA and OLA ligands. **c**, Photographs of Pt, Pd and Fe_3O_4 NCs in toluene. These NCs were recovered from $AlCl_3/AlCl_4^-$, redispersed in toluene with additional organic ligands, and purified with toluene/ethanol. **d**, Fourier transform infrared (FTIR) spectra of Pt NCs with organic ligands (black) and recovered from $AlCl_3/AlCl_4^-$ (red). The absence of vibrational peaks of original organic ligands (for example, C–H stretching at $2,800$–$3,000\,cm^{-1}$) suggests that NCs dispersed in $AlCl_3/AlCl_4^-$ are free of organic ligands at the surface[6]. We speculate that $[Al_2Cl_7^-]$ (and the minor Al_2Cl_6 and $AlCl_3$), a very strong Lewis acid,

plays a similar role to Me_3O^+ in Me_3OBF_4 as the ligand-stripping agent[7]. As a consequence, NCs with both organic-ligand-capped surfaces (using a phase transfer method) and bare surfaces could be well stabilized in $AlCl_3/AlCl_4^-$. **e**, FTIR measurements of CdSe/CdZnS core/shell QDs recovered from the dispersion in NaSCN/KSCN show a shift of the SCN^- peak to higher frequencies (from $2,060$ to $\sim2,090\,cm^{-1}$) compared to pure NaSCN/KSCN. According to ref. 16, $Cd(SCN)_2$ powders and SCN^--capped CdSe NC solids show characteristic SCN^- stretching peaks at $2,100$–$2,150\,cm^{-1}$, which are at higher frequencies compared to NaSCN and KSCN. Thus, the observed shift was probably due to the formation of Cd– or Zn–SCN complexes at the QD surface.
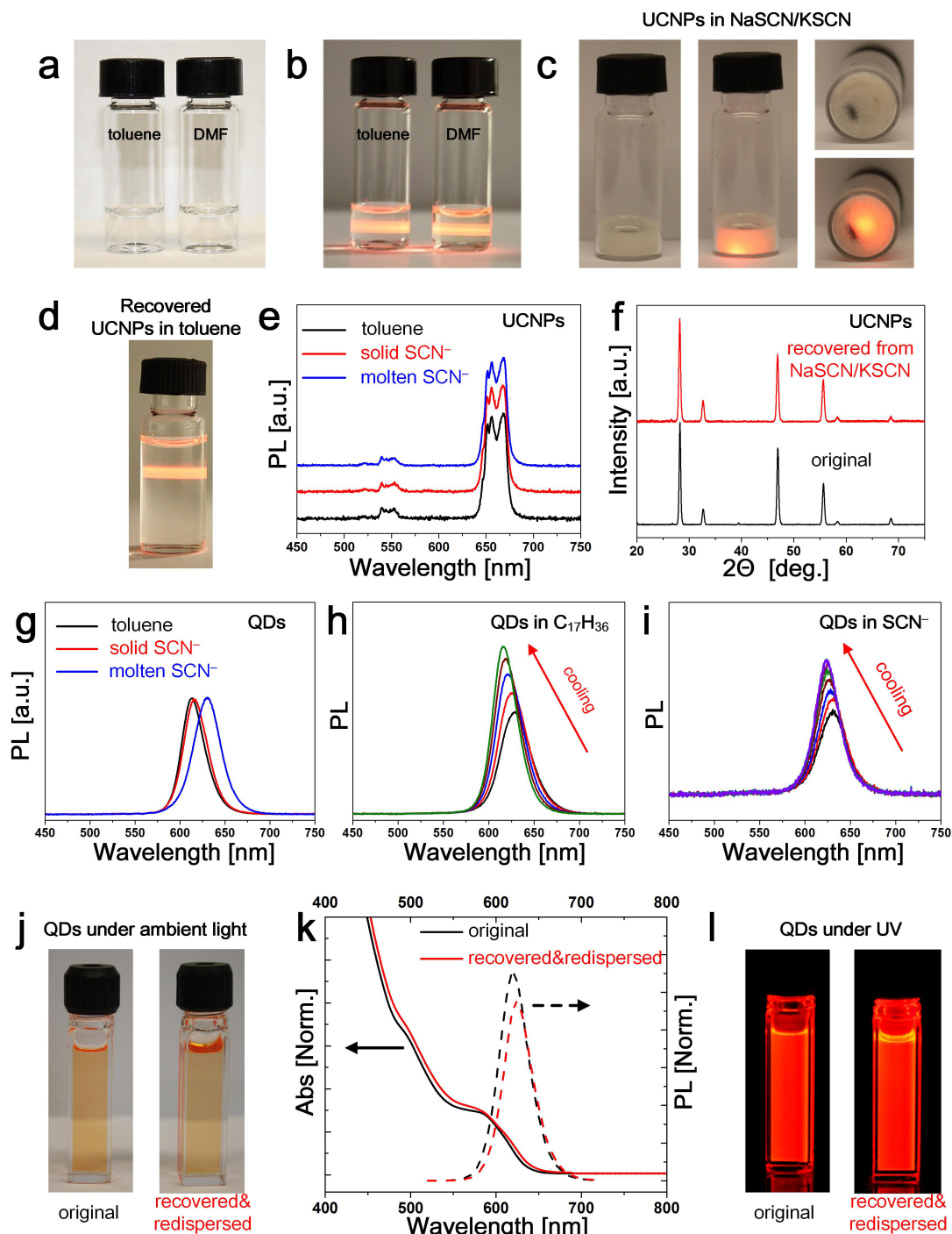
Extended Data Figure 3 | Stability and photoluminescence (PL) of nanocrystals in molten salts. a, b, Stable colloids of UCNPs in toluene (with OA ligands) and in DMF (bare NCs treated by NOBF$_4$) under ambient light (**a**) and illuminated by a 980 nm near-infrared (IR) laser beam (**b**). An orange emission was observed under IR illumination for both solutions. **c,** Photographs of a solidified UCNP/NaSCN/KSCN composite under ambient light (left panel and top right panel) and illuminated by a 980 nm near-IR laser (middle panel and bottom right panel). The orange emission from UCNPs was preserved. The dark object at the bottom of the vial (shown in the right panels) is the stir bar. **d,** Photograph of UCNPs recovered from NaSCN/KSCN and redispersed in toluene with additional OA, showing an orange emission under IR illumination. **e,** PL spectra of UCNPs in toluene and in NaSCN/KSCN (SCN$^-$) in both solid and molten states. **f,** The X-ray diffraction

(XRD) patterns of original UCNPs and UCNPs recovered from NaSCN/KSCN. No change in the XRD pattern is observed. **g,** PL spectra of CdSe/CdZnS QDs in toluene and NaSCN/KSCN (SCN$^-$) in both solid and molten states. **h, i,** The temperature dependence of PL spectra of QDs in heptadecane (C$_{17}$H$_{36}$; **h**) and SCN$^-$ (**i**). In both cases, the samples were preheated at 150 °C and allowed to cool down. The red-shifted PL peak at high temperatures was observed in both C$_{17}$H$_{36}$ and SCN$^-$ because of the reduced bandgap. **j, l,** Photographs of original and recovered/refunctionalized QDs in toluene solution under ambient (**j**) and UV (**l**) light. **k,** Absorption (solid lines) and emission (dashed lines) spectra of QDs with original organic ligands (black) and the ones recovered from NaSCN/KSCN and re-functionalized by OA (red). Minimal changes in the absorption spectra and a slight decrease of PL efficiency were observed after dispersing QDs in molten NaSCN/KSCN for several days.
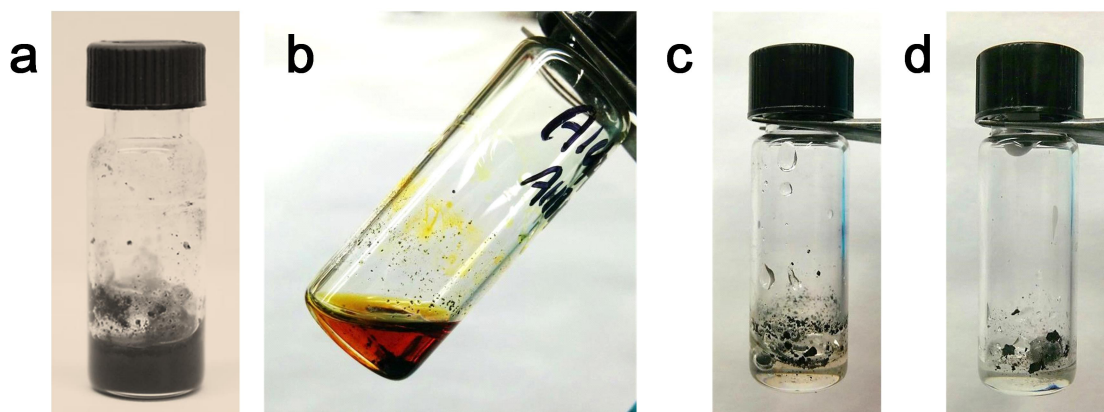
Extended Data Figure 4 | Unstable NC suspension in Lewis neutral salts. a–d, Photographs of unstable, inhomogeneous mixtures of Pt NCs in **a,** $AlCl_4^-$, **b,** $AlCl_4^-/AlBr_4^-$, **c,** NO_3^- and **d,** NO_3^-/NO_2^-. Pt NCs undergo severe agglomeration owing to the lack of repulsive force. See Extended Data Table 1 for a full list of the components of the salts.
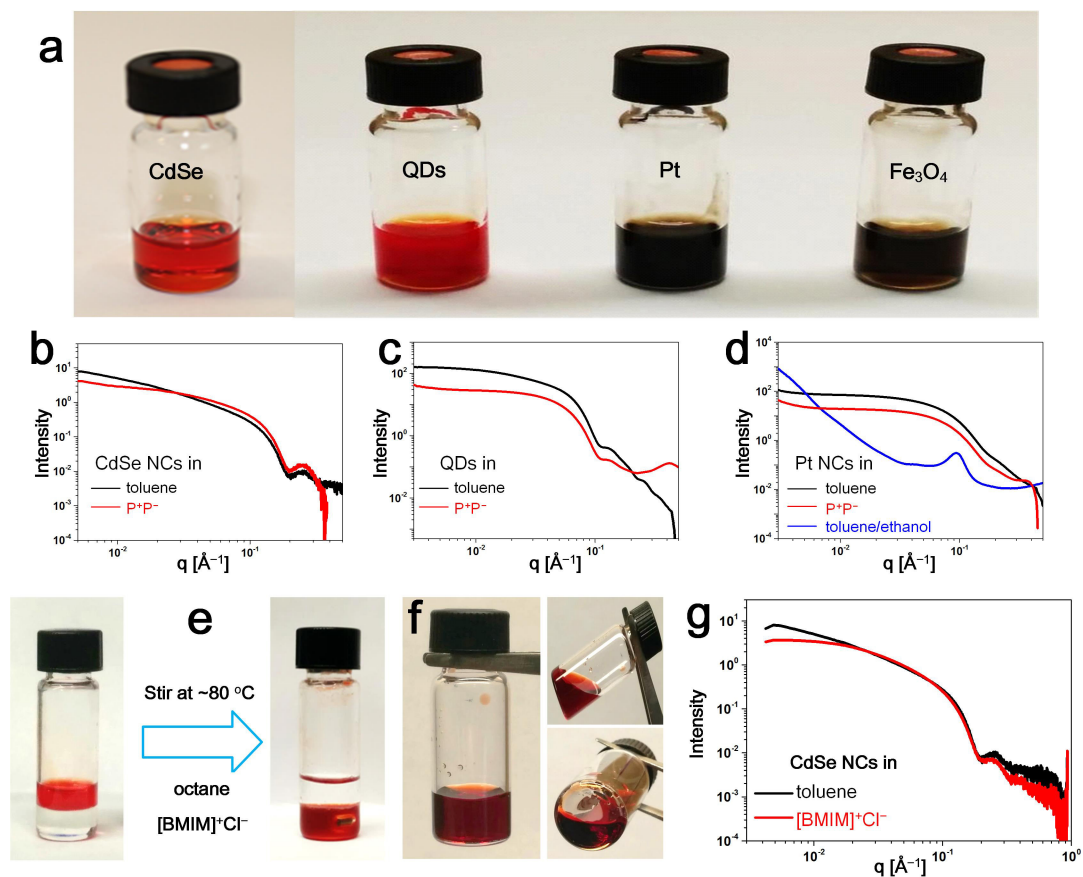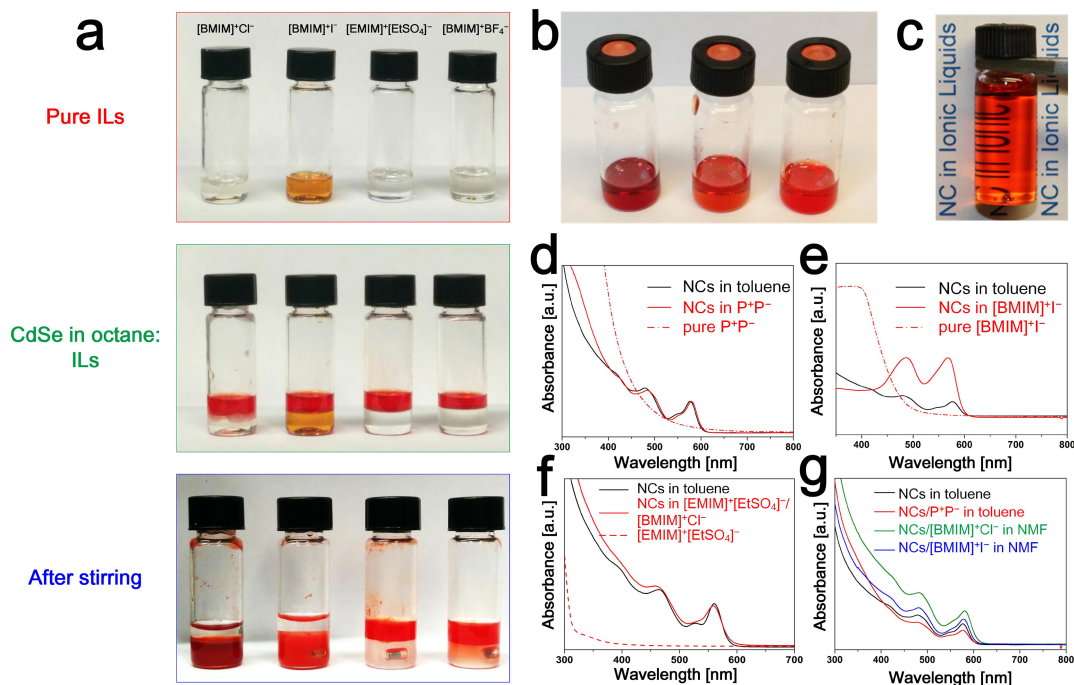
**Extended Data Figure 5 | Stable NC colloids in ionic liquids.**
a, Photographs of stable NC colloids in P^+P^- (Methods). **b–d**, Small-angle X-ray scattering (SAXS) patterns of CdSe (**b**), QDs (**c**) and Pt NCs (**d**) in toluene and P^+P^-. The SAXS patterns of NCs in P^+P^- resemble those of NCs in toluene, indicating high NC colloidal stability. **e**, Photographs showing the phase transfer of CdSe NCs from octane to $[BMIM]^+Cl^-$ without additional ligands. **f**, Photographs of stable CdSe NC colloids in $[BMIM]^+Cl^-$. **g**, SAXS patterns of CdSe NCs in toluene (with OA/TOP/TOPO) and in $[BMIM]^+Cl^-$. All samples were gently heated to keep $[BMIM]^+Cl^-$ in the molten state.

Extended Data Figure 6 | CdSe NC colloids in imidazolium-based ionic liquids. Figure shows the effect of anions in ionic liquids on colloidal stability and the absorption features of nanocrystal colloids. **a**, Photographs showing the phase transfer of CdSe NCs. Top, pure ILs; middle, biphasic systems with CdSe NCs in octane as the top layer and the ILs as the bottom layer; bottom, CdSe NCs transferred from octane to Lewis basic $[BMIM]^+Cl^-$ and $[BMIM]^+I^-$. In comparison, no phase transfer was observed in the Lewis neutral $[EMIM]^+[EtSO_4]^-$ or $[BMIM]^+BF_4^-$. Photographs of **b**, stable colloids of CdSe NCs in (from left to right) $[BMIM]^+Cl^-$, $[EMIM]^+[EtSO_4]^-$ with added $[BMIM]^+Cl^-$, and $[EMIM]^+[EtSO_4]^-$ with added $[BMIM]^+I^-$ and **c**, a stable colloid of CdSe NCs in $[BMIM]^+BF_4^-$ with added $[BMIM]^+Cl^-$. Adding a small amount of surface-binding chloride or iodide ions to $[BMIM]^+BF_4^-$ or $[EMIM]^+[EtSO_4]^-$ resulted in a stable CdSe NC colloid (**b, c**) free of the original organic ligands. **d–g**, UV–visible absorption spectra of CdSe NCs in various ILs and their mixtures with organic solvents. Shown for NCs in **d**, P^+P^-, **e**, $[BMIM]^+I^-$, **f**, $[EMIM]^+[EtSO_4]^-$ with a small amount of $[BMIM]^+Cl^-$, and **g**, ILs diluted with toluene or NMF. The absorption spectra of pure ILs and CdSe NCs in toluene are given for reference.
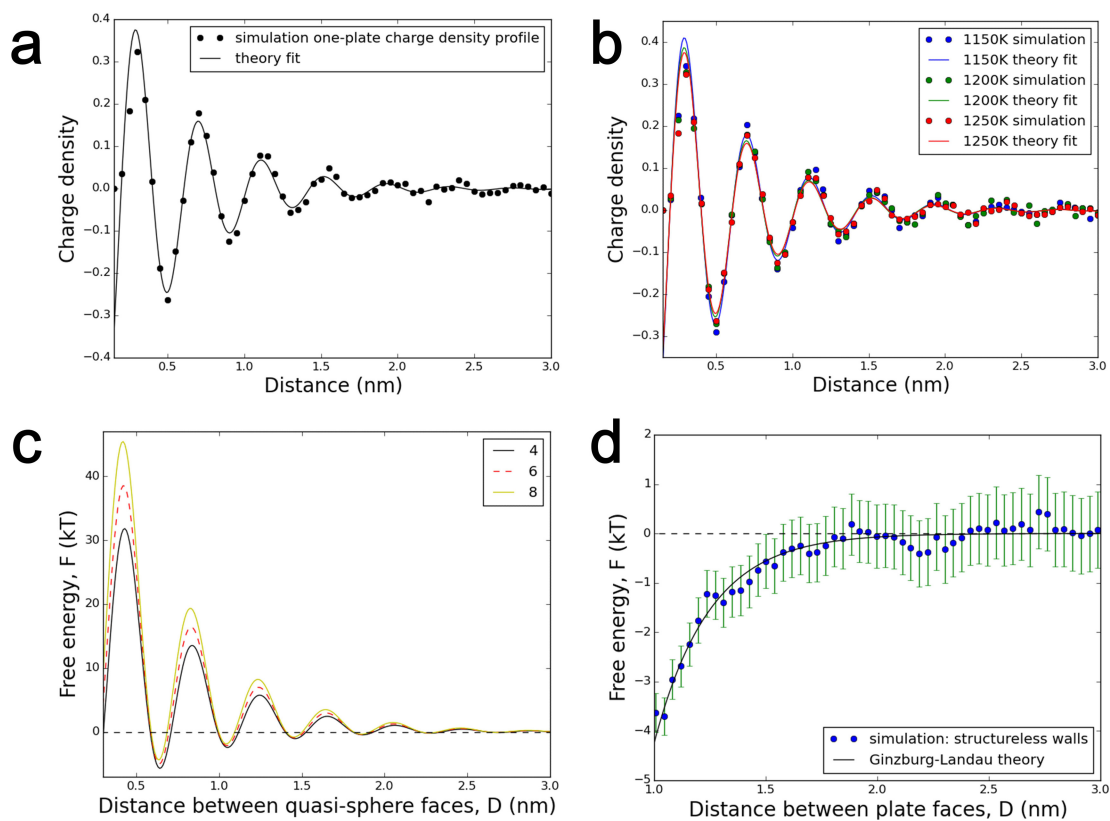
Extended Data Figure 7 | Simulations of CdSe surface in molten KCl.
a, Simulated charge density profile as a function of the distance away from the [001] surface of a CdSe nanocube (2.45 nm × 1.85 nm × 1.85 nm) in molten KCl (black dots) and the fit with Ginzburg–Landau theory (solid line). The charge density is defined as $[n_+(D) - n_-(D)]/n_s$, where $n_-(D)$ and $n_+(D)$ are the densities of Cl^- and K^+ at the plane of D while n_s is the total ion density. **b**, Simulated charge density profiles around a CdSe nanocube sized as in **a** in molten KCl, and the corresponding fits at various temperatures above the melting point of KCl. **c**, Simulated free energy of layering between two quasi-spherical CdSe NCs (10 nm in diameter) in molten KCl. The quasi-spheres are formed by one parallel facet and 4, 6 or 8 tilted facets (see Supplementary Discussion for more details). **d**, Simulated free energy of layering between two structureless (or chemical inert) walls in molten KCl (blue dots) and the fit by Ginzburg–Landau theory (black curve). Error bars in **d** are related to state-state covariance as discussed elsewhere[35] (see Supplementary Discussion for additional details).

Pt NCs in Ga–In   Pt NCs in Wood's alloy
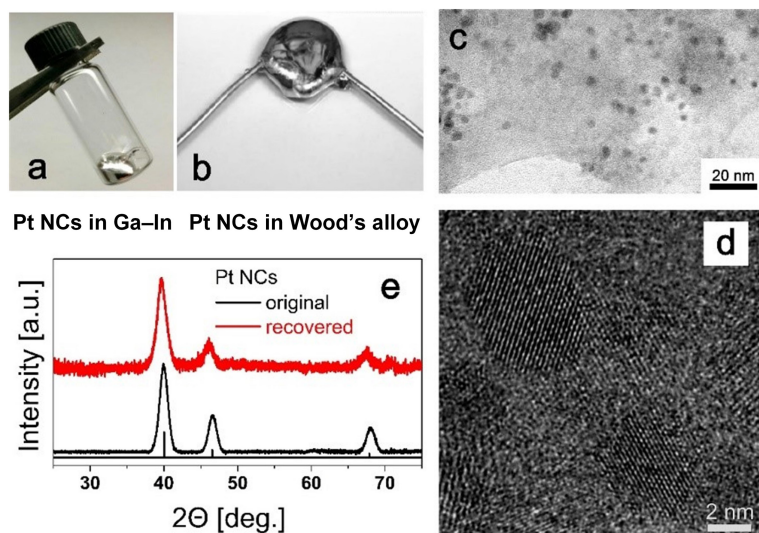
Extended Data Figure 8 | Nanocrystal colloids in liquid metals.
a, Photograph of a dispersion of ligand-stripped Pt NCs in liquid Ga–In eutectic ($T_m \approx 15.5\,°C$). Pt NCs were homogeneously distributed in the metal matrix with a concentration of $\sim 4\,mg\,ml^{-1}$, as indicated by ICP–OES analysis. **b**, Photograph of two metal wires soldered by a piece of Wood's metal (50% Bi, 26.7% Pb, 13.3% Sn and 10% Cd by weight, $T_m \approx 70\,°C$) containing Pt NCs. **c**, **d**, TEM (**c**) and high-resolution TEM (**d**) images of Pt NCs in a thin layer of Ga–In eutectic, showing that the NCs retain their integrity and are uniformly distributed throughout the metal matrix. **e**, Powder XRD pattern (traces) of original Pt NCs and NCs recovered from Ga–In. The line pattern (bottom) shows the diffraction peaks for the bulk fcc Pt phase.
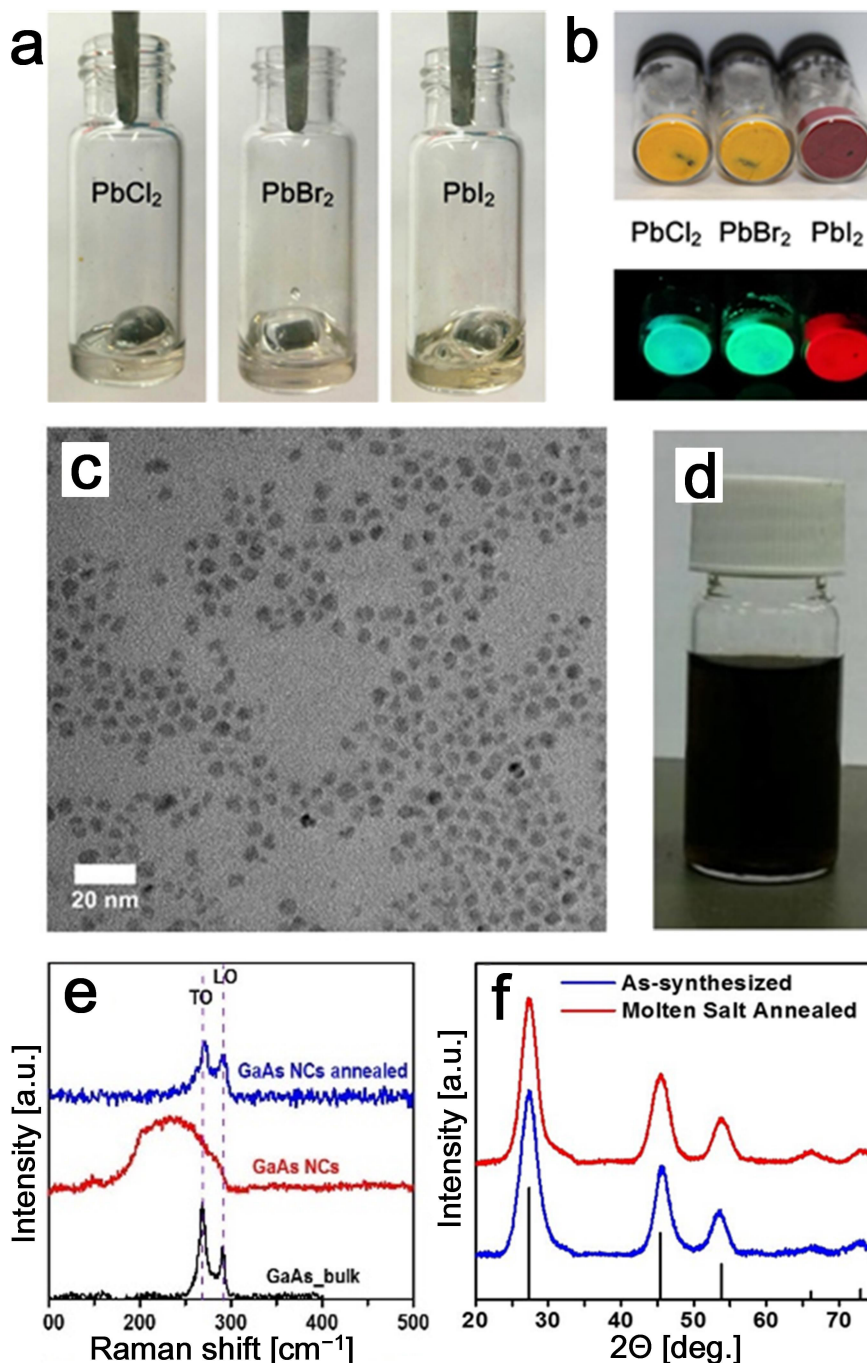
Extended Data Figure 9 | Colloidal synthesis and chemistry in molten inorganic salts. a, Photographs of PbX_2 (X = Cl, Br, I) in molten CsBr/LiBr/KBr. In each salt mixture, PbX_2:CsBr = 0.03 mol%. **b**, Solidified PbX_2 in CsBr/LiBr/KBr under ambient (top) and UV light (bottom). Adding PbX_2 (X = Cl, Br, I) to CsBr/LiBr/KBr resulted in the formation of colourless (mixed) compounds in the molten state (**a**). On solidification, the (mixed) compounds showed vivid colours and strong PL under UV light. This indicates the formation of emissive, ternary or quaternary alkali lead halides in molten salt. **c**, TEM image of GaAs NCs and **d**, a photograph of GaAs colloidal solution. **e**, Raman spectra of bulk GaAs (black), as-synthesized (275 °C) GaAs NCs (red) and GaAs NCs annealed at 500 °C using a CsBr/LiBr/KBr molten salt as the solvent (blue). **f**, XRD patterns of as-synthesized and annealed GaAs NCs prepared as in **e**. GaAs NCs formed a stable colloid in molten CsBr/LiBr/KBr when using a 'solvent-free' method. After annealing in the inorganic salt solvent at 500 °C, the quality of the GaAs NCs was significantly improved, as indicated by the well-defined TO and LO modes in **e**, while the NC size was preserved (**f**).

Extended Data Table 1 | Experimentally tested combinations of NCs and molten inorganic salts or ILs forming homogeneous colloids

Formula (mol.%)	Abbreviation	T_m (°C)*	Nanocrystals†
$AlCl_3$:$NaCl$:KCl = 63.5:20:16.5	$AlCl_3$/$AlCl_4^-$‡	~90	Pt, FePt, Pd, QD, UCNPs with organic surfactants (up to ~30); bare FePt, QD, UCNPs, and Fe_3O_4 NCs (up to ~30)
$AlBr_3$	$AlBr_3$	97.8	Pt, FePt, Pd NCs with organic surfactants (up to ~20)
$KSCN$:$NaSCN$ = 73.7:26.3	SCN^-	130–140	Bare QD, UCNPs, FePt NCs (up to ~50)
$LiCl$:LiI:KI = 2.6:57.3:40.1	Cl^-/I^-	270	Bare InP, UCNPs (up to 50)
$LiCl$:$LiBr$:KBr = 25:37:38	Cl^-/Br^-	320	Bare InP, UCNPs (~20)
$CsBr$:$LiBr$:KBr = 25:56.1:18.9	Br^-	230	Bare InP, UCNPs (up to 50)
$ZnCl_2$:$NaCl$:KCl = 60:20:20	$ZnCl_2$/$ZnCl_4^{2-}$	203	Bare InP, UCNPs (~20)
$LiAlBr_4$:$NaAlCl_4$:$KAlCl_4$ = 30:50:20	$AlCl_4^-$/$AlBr_4^-$	86	No stabilization
$NaAlCl_4$:$KAlCl_4$ = 70:30	$AlCl_4^-$	129	No stabilization
$NaNO_3$:KNO_3:$LiNO_3$:$Ca(NO_3)_2$:$CsNO_3$ = 6:23:8:19:44 (wt.%)	NO_3^-	65	No stabilization§
$NaNO_3$:KNO_3:$LiNO_3$:$NaNO_2$ = 14.2:50.5:17.5:17.8 (wt.%)	NO_3^-/NO_2^-	100	No stabilization
trihexyl(tetradecyl)phosphonium bis(2,4,4-trimethylphenyl)phosphinate	P^+P^-	/	CdSe, QDs, Pt, FePt, Fe_3O_4 NCs with organic surfactants (~50 mg/mL)
1-butyl-3-methylimidazolium chloride	$[BMIM]^+Cl^-$	~73	CdSe (~50), QDs (20) via phase transfer
1-butyl-3-methylimidazolium iodide	$[BMIM]^+I^-$	/	CdSe (30) NCs via phase transfer
1-butyl-3-methylimidazolium tetrafluoroborate or 1-ethyl-3-methylimidazolium ethylsulfate	$[BMIM]^+BF_4^-$ or $[EMIM]^+[EtSO_4]^-$	/	No phase transfer or stabilization for NCs with organic surfactants

*Melting points (T_m) of molten inorganic salts may vary slightly in different literature sources.
†Numbers in parentheses indicate the solubility limits of nanocrystals from preliminary screening experiments (in units of mg ml^{-1}).
‡Mainly contains $[AlCl_4^-]$ and $[Al_2Cl_7^-]$ with Na^+ and K^+, and minor species Al_2Cl_6 and $AlCl_3$ (ref. 13).
§The only prior publication related to stable nanoparticle colloids in a molten inorganic salt was published in 1969 and described the synthesis of metastable Au sols in eutectic nitrate mixtures[37].